www.nature.com/scientificreports

scientific reports

OPEN

Differentiation of canine and feline neoplasms using multi-modal imaging and machine learning

Martynas Maciulevičius[1,2,3,4]✉, Greta Rupšytė[3]✉, Renaldas Raišutis[3,5], Blaž Cugmas[4] & Mindaugas Tamošiūnas[1,4]

Canine/feline (sub-)cutaneous tumors, which include lipomas, mastocytomas and soft tissue sarcomas, introduce diagnostic challenges due to inherent tissue heterogeneity, accompanied by diverse clinical pathogenesis. Current study integrates conventional imaging techniques optical (white light and autofluorescence) as well as high frequency ultrasound imaging to train machine learning classifiers: linear discriminant analysis, support vector machine and random forest. Study resulted in ~100% classification efficiency between benign lipoma and combined mastocytoma and sarcoma tissues for all the classifiers. For the differentiation between mastocytoma and sarcoma tumors, both support vector machine and random forest outperformed conventional linear discriminant analysis classifier. Support vector machine displayed the highest classification efficiency for bimodal groups: (i) ultrasound + fluorescence and (ii) ultrasound + white light as well as (iii) fluorescence + white light. However, it failed for trimodal ultrasound + optics combination, indicating possible upper limit for imaging mode addition. The multimodal effect was obtained using both statistically significant set of features as well as optimal set of features, determined using sequential feature addition. Resulting classification efficiency for combined ultrasound + fluorescence approach was > 85% and even higher for ultrasound + white light or ultrasound + optics multimodal approaches reaching ~ 95%. In the classification of mastocytoma and sarcoma, support vector machine classifier was able to detect significant ($p < 0.05$) multimodal effect for bimodal groups of: (i) fluorescence + white light, (ii) ultrasound + fluorescence and (iii) ultrasound + white light. On the contrary, random forest demonstrated relevant increment only for the combination of fluorescence and white light. Inferior features of ultrasound or fluorescence have been evaluated to be competitive with the features of highly-efficient white light as they were automatically selected during the process of feature optimization. In addition, another phenomenon of manifestation of multimodality has been observed: in multimodal groups, ultrasound features tended to substitute the features of white light, not just simply be added to them. Multimodal approach was determined to be highly-required for the classification of heterogeneous mastocytoma and sarcoma tumors, which display more similar morphological characteristics. However, when differentiating very distinct lipomas from mastocytomas or sarcomas, the multimodal approach was not a requisite.

Keywords Optical imaging, Fluorescence imaging, Ultrasound imaging, Sarcoma, Mastocytoma, Multimodal diagnostics

The most common skin and subcutaneous tumors among canine/feline neoplasms are soft tissue sarcomas (STS, 20.3%), mast cell tumors (MCT, 16.8%) and lipomas (LPs, 8.5%)[1]. Accurate and precise diagnosis of these tumors is essential for the selection of appropriate therapeutic strategy, leading to efficient animal recovery. MCTs are very heterogeneous and range from benign to malignant, whereas STSs are characterized as aggressive and malignant. Therefore, they both introduce significant diagnostic challenges mostly inherent to their structural

[1]Research Institute of Natural and Technological Sciences, Vytautas Magnus University, Universiteto 10, LT-53361 Akademija, Kaunas District, Lithuania. [2]Department of System Analysis, Faculty of Informatics, Vytautas Magnus University, Universiteto str. 10–213, LT-53361 Akademija, Kaunas District, Lithuania. [3]Ultrasound Research Institute, Kaunas University of Technology, K. Baršausko st. 59, LT-51423 Kaunas, Lithuania. [4]Institute of Atomic Physics and Spectroscopy, University of Latvia, Jelgavas st. 3, Rīga LV-1004, Latvia. [5]Department of Electrical Power Systems, Faculty of Electrical and Electronics Engineering, Kaunas University of Technology, Studentų St. 48, LT-51367 Kaunas, Lithuania. ✉email: martynas.maciulevicius@vdu.lt; greta.rupsyte@ktu.lt

diversity[2–4]. Traditional diagnostic methods, such as histopathology or cytology, although effective, are time-consuming and often subjective.

Unlike in human cutaneous malignancies, where certain skin tumors can be assessed by dermatoscopy, veterinary oncologists are limited to an invasive diagnostic method, called fine-needle aspiration cytology (FNAC). The efficiency of FNAC in detecting malignant skin and subcutaneous tumors can be low, as reported in the recent study by Wang et al. – 77.2% specificity and 68.6% sensitivity[5]. Consequently, this results in a large number of undiagnosed cases, therefore, veterinarians need reliable and straightforward screening techniques for cancer detection. For this reason, the techniques of optical imaging have been explored. Among them, optical coherence tomography (OCT) has emerged as a leading technology, mainly, due to its ability to delineate tumor margins for different cancer types. This includes research on MCT and STS tumors in canines[4,6] as well as STSs in felines[7]. There are studies employing OCT for the efficient differentiation between STSs and healthy tissues in dogs [4] as well as between LPs and combined set of MCTs and STSs in both cats and dogs[8]. However, OCT was reported to be not that reliable for tissue differentiation, as it possesses certain limitations such as: challenging image interpretation, few-millimeter imaging depth and typical axial resolution of > 10 μm[9]. Therefore, OCT has been incorporated into hybrid diagnostic approach with Raman spectroscopy to enhance its effectiveness[8]. However, OCT as well as Raman are a high-cost modern devices, usually unaffordable for conventional veterinary clinics.

Recent advances in digital imaging, accompanied by machine learning (ML), have paved the way for analytical algorithms, capable to handle large datasets of imaging data. This allowed for the integration of different conventional imaging modes leading to diagnostic synergism. Since, each of them provides different morphological information, their combination usually allows to surpass the diagnostic efficiency of a single cutting-edge machine. By combining imaging data with computational techniques, the sets of quantitative textural features, indicative of tumor surface morphology as well as internal structure, are attained. Hence, there is a growing interest in the integration of easy-to-access diagnostic modalities, such as, optical and ultrasound (US) imaging. The latter a capable to provide real-time and high-resolution insights into tumor morphology, architecture and composition[10].

In dogs and cats, US has already been tested for the detection of superficial tumors. Despite the changes in vascularity and perfusion between benign and malignant tumors, efficient tumor differentiation remained challenging, mostly due to significant similarities observed in acoustic characteristics of the tumors[10]. Real-time elasto-sonography has recently shown better potential (100% sensitivity, 61–89% specificity) to distinguish between benign LP and malignant tumors, based on tissue softness/hardness[11]. However, the expertise of radiologist was still required. Also, due to small tumor size, low US resolution was indicated as a decisive drawback.

In the current study, we have employed scanning acoustic microscopy (SAM) – a technique that has been used in other studies and yielded promising and innovative results. Miura et al. used SAM (80–120 MHz) to differentiate between normal, neoplastic and inflammatory tissues based on the speed of sound[12]. In addition, SAM (760 MHz) was used to assess arterial stiffness in the aortic biopsy. The patients with elevated cholesterol or glucose levels were associated with higher US velocities, suggesting a correlation between arterial stiffness and metabolic data[13].

Our study focuses on multimodal imaging using SAM, white light (WL) and autofluorescence (FL) imaging on hematoxylin and eosin (H&E)-stained histological samples. FL imaging provides complementary data on biochemical and structural tissue composition, usually overlooked by WL imaging. Eosin's FL is detected in green-yellow spectral region (~ 520–550 nm) when excited by light of 490–520 nm wavelength[14]. Eosin stains the components of the extracellular matrix, such as collagen and muscle fibers, clearly visible in FL images[15]. FL in combination with diffuse reflectance spectroscopy has significantly enhanced the detection rate of oral malignant lesions from normal tissue[16]. Also, by highlighting collagen structures, it enhanced the diagnostic accuracy of breast cancer as well as identified brain tumors in the loci of low visibility, according to the fluorescence of 5-aminolevulinic acid (5-ALA)[17,18].

Aim of our study – to develop a new ML-based strategy, capable to provide automated differential diagnosis of veterinary (sub-)cutaneous cancer in real-time. The proposed technology is based on the techniques of multimodal imaging, combining optical (WL and FL) as well as high frequency (360 MHz) US data. Tissue classification employs ML classifiers: linear discriminant analysis (LDA), support vector machine (SVM), decision tree (DT) and random forest (RF). Such a novel combination of hybrid optical (high resolution, low penetration) and US (low resolution, high penetration) imaging modalities can lead to a competitive technique compared to conventional high-cost diagnostic devices. Therefore, our approach shows potential to:

(i) improve diagnostic accuracy of ex vivo as well as intraoperative veterinary skin cancer;
(ii) improve early-stage diagnostics of skin malignancies in veterinary patients by reducing the number of unnecessary surgeries and improving pet health;
(iii) provide a real-time ML-based diagnostic back-up for veterinary histopathologists.

Materials and methods

Veterinary patients

Study was conducted according to guidelines and regulations under permission No. DZLAEP-2021/3 of the Ethical Council of Animal Welfare and Protection (Latvia University of Life Sciences and Technologies, Jelgava, Latvia). Informed consent was obtained from all pet owners. Animal procedures were carried out in accordance with ARRIVE guidelines.

18 LP tumors were collected from 13 veterinary patients (11 dogs and 2 cats), 30 STS tumors – from 23 patients (12 dogs and 11 cats) as well as 18 MCT tumors from 15 patients (12 dogs and 3 cats). The average age

of animals was 8.3 years (in overall, 2–13 years). Additional details about the tumors are given in Appendix_ Table_1. After surgical dissection, ex vivo tumor samples were kept in formalin solution (10%). Subsequently, tumors were microscopically sectioned and histologically stained (H&E) to obtain histological samples.

US and optical imaging

US imaging. EasySAM acoustic microscope (Kibero, Germany) was used for the scanning of histological slides (Fig. 1). Three dimensional (3-D) (200 × 200 × 512) data arrays of 200 × 200 radio-frequency signals were acquired; each signal consisted of 512 samples, registered at 2×10^9 sample/s sampling rate. The peak temporal amplitude of each radio-frequency signal was generated using a summation algorithm, which yielded the grayscale color value for a single pixel in the US image with a 10 µm resolution.

Optical imaging. WL imaging was carried out using a Pannoramic 250 FLASH III DX bright-field scanner (3DHistech Kft., Budapest, Hungary), equipped with a 20×/0.8 NA Plan-Apochromat (Carl Zeiss, Germany) objective (Fig. 1) and FL channels. WL images, obtained for each tumor, were evaluated by experienced veterinary histopathologist to provide the diagnosis. Autofluorescence images were registered via yellow fluorescence channel (YFL, Cy3). Excitation was performed using 531/40 nm wavelength light source, emission was detected using 590/40 nm band-pass filter with a resolution of 0.121 µm/pixel.

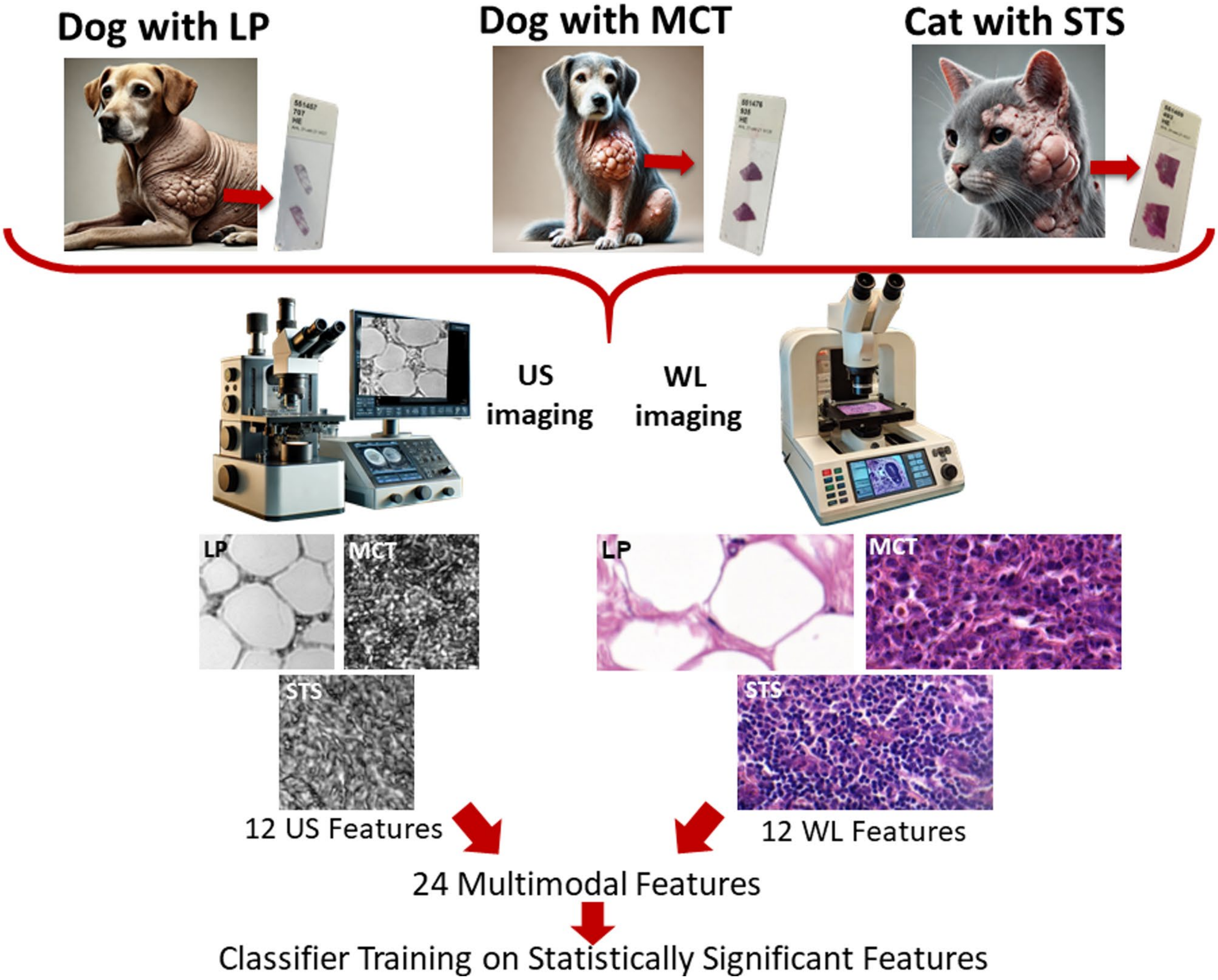

Fig. 1. Illustration of the first part of the study. Histological samples obtained from veterinary patients were used to acquire US and WL images. Subsequently, 12 morphological features were quantified for US and WL images, resulting in separate feature datasets for US, WL and combined, US + WL, groups. Statistically significant features were used to train ML algorithms to derive the essential metrics, representing the efficiency of tissue classification. Illustrations of hypothetical tumor-bearing animals and US/optical scanners were generated using DALL·E image generation software (OpenAI, version 2; https://openai.com/dall-e). Other images were created by the authors.

US data analysis

A total of 6 STS, 10 LP and 10 MCT US C-scans were derived for each tumor. Since, there were 30 STS, 18 LP and 18 MCT tumors, this data arrangement resulted in 180 US images for each neoplasm class. Spectral analysis (fast Fourier transform, FFT) as well as temporal analysis were performed for each US radio-frequency signal, corresponding to a pixel, located within the 3-D array (Fig. 2). This produced different US colormaps: (i) Attenuation; (ii) Phase Change; (iii) Frequency at Peak FFT Amplitude (Peak FFT Freq); (iv) Value of Peak FFT Amplitude (Peak FFT Amp); (v) Peak Temporal Amplitude (Peak TEMP Amp); (vi) Minimal Temporal Amplitude (Min TEMP Amp) (Fig. 2). Each US colormap was saved separately as an image in TIFF format.

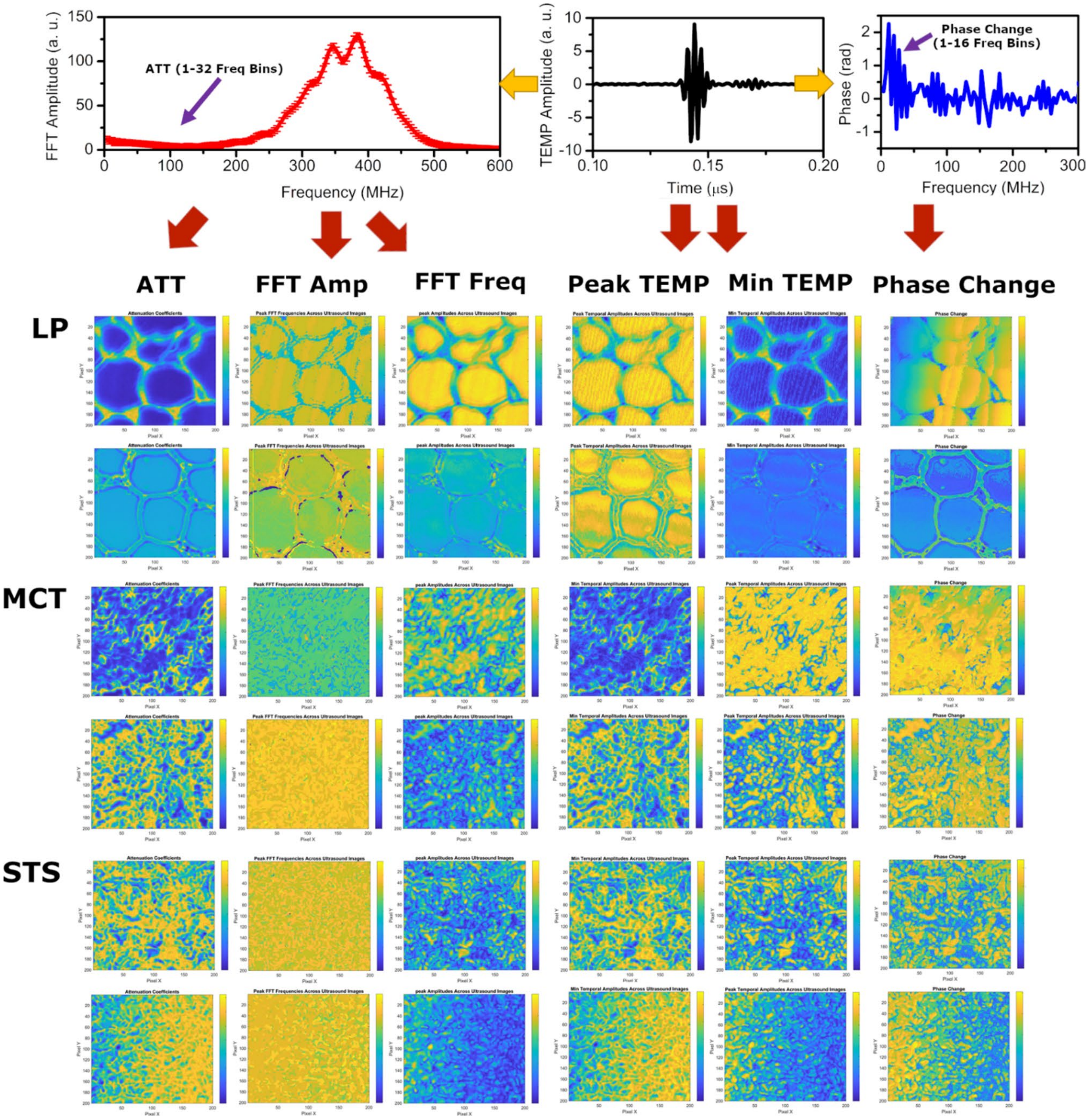

Fig. 2. Attenuation, quantified in 3.9–125 MHz frequency range (1–32 Freq Bins), Peak FFT Freq and Peak FFT Amp were quantified using the data of FFT amplitude spectrum of US radio-frequency signals (columns 1–3). Peak TEMP Amp and Min TEMP Amp were determined from temporal domain of the acoustic signals (columns 4–5). Phase Change was quantified in 3.9–62.5 MHz frequency range (1–16 Freq Bins) using the data of FFT phase spectrum (column 6). Eventually, 12 morphological features were quantified for each group of US colormaps.

High frequency US imaging effectively visualized the overall structure of LPs, displaying the lobular honeycomb composition. US images of MCTs and STSs revealed dense and irregular internal structure, opposite to homogeneous LP.

Optical data analysis

6 STS, 10 LP and 10 MCT regions of interest (ROIs) (1500 × 800 pixels) containing cancerous tissue, were subtracted from the original image for the analysis (Fig. 3). The procedure of ROI selection in cancer loci is demonstrated in Appendix_Figs._1–3. This was performed due to alternating loci of healthy and cancerous tissue within FL and WL images. It resulted in 180 ROIs for each tissue class: LP, MCT and STS. The described procedure for WL images (the same tumor) was repeated twice - in order to obtain two datasets: WL1 and WL2. This was done to: (i) arrange a more competitive set of optical features (36) in comparison to US (72), and (ii) account for tissue heterogeneity, since WL2 resulted in slightly higher differentiation efficiency. Each image patch (ROI) was saved separately as TIFF image.

WL imaging provided high-resolution images, representing the patterns of surface morphology of different tumors (Fig. 3). In general, WL imaging provided the initial assessment of the tissues and identified superficial abnormalities. LPs were very distinct with typical honeycomb structure, whereas MCTs and STSs exhibited more similar dense surface characteristics. The presence of tissue heterogeneity within single MCT or STS class was also significant. FL imaging highlighted the stromal composition within tissues; also, it was capable to enhance cell-to-cell contrast for MCTs. However, optical imaging has limitation in visualizing deeper structures, therefore, it was combined with US imaging.

Extraction of morphological features

Quantitative features, computed to acquire the inherent characteristics of the particular tissue class were: (1) Entropy, (2) Contrast, (3) Correlation, (4) Energy, (5) Homogeneity, (6) Average, (7) Standard deviation (SD), (8) Root mean square (RMS), (9) Variance, (10) Smoothness, (11) Kurtosis, (12) Skewness[19].

Features such as entropy, average, SD, RMS, variance, smoothness, kurtosis, skewness define the overall distribution of the intensity of pixels within the image[20]. Other features: contrast, correlation, energy, homogeneity were computed using grayscale co-occurrence matrix to provide textural characteristics of the image[21].

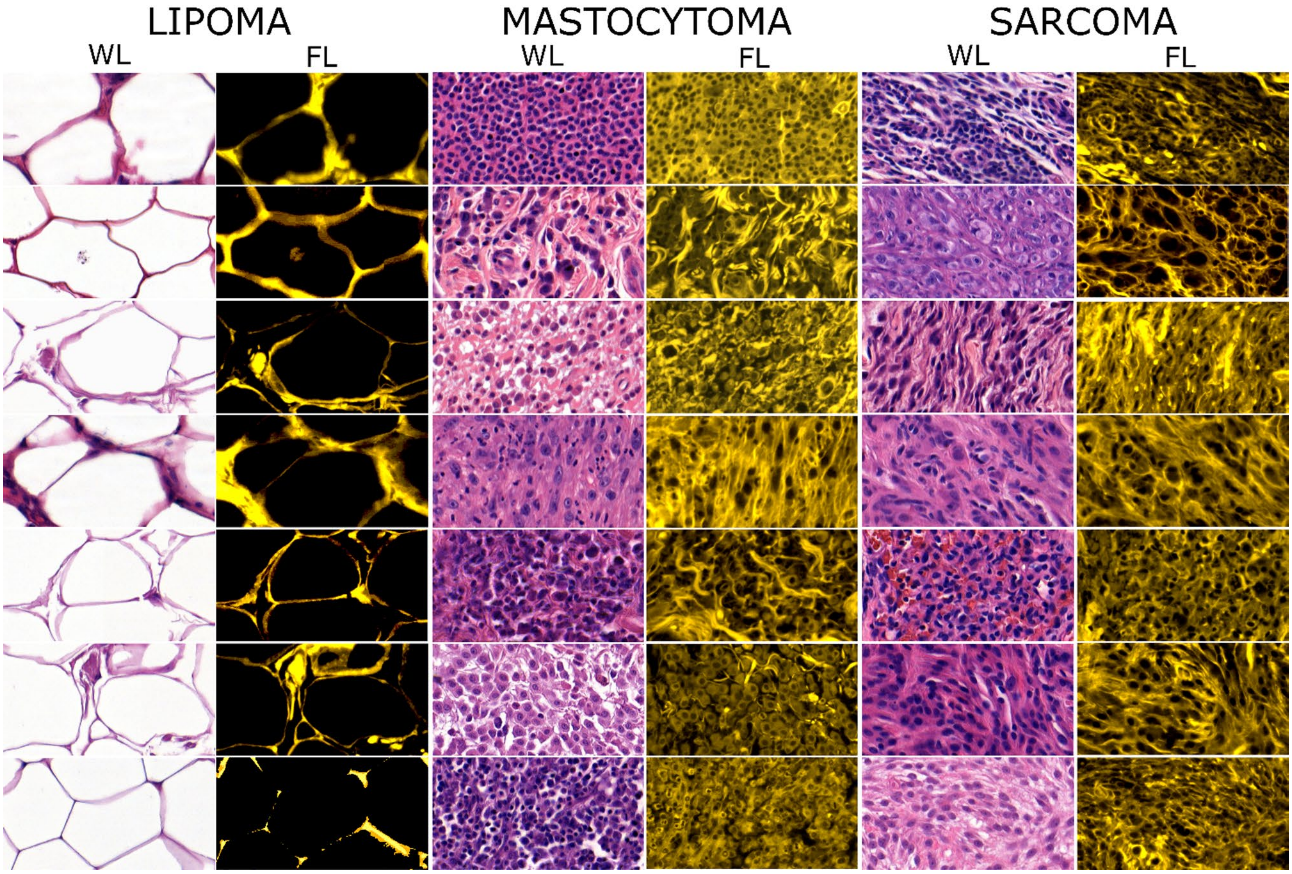

Fig. 3. Optical images of LP, MCT and STS. Columns 1, 3 and 5 indicate WL images, correspondingly, columns 2, 4 and 6—FL images. 12 morphological features were quantified for each tissue class.

Classifier training

Classifiers

LDA. Classifier was implemented using a linear discriminant type with a 'uniform' function, to ensure that each class has equal weight during the classification process. Equal feature contribution to the classifier, despite different ranges/ units, was achieved by feature normalization by min-max [0;1] scaling. Normal distribution of features was determined for 84.3% (273/324) of cases (Kolmogorov-Smirnov test); homogeneity of variance – for 88.8% (288/324) of cases (Brown-Forsythe test). The minimal level of statistical significance (p) was set to < 0.05.

SVM. During data pre-processing, the standardization of features was performed. Classifier was implemented with RBF (radial basis kernel) function, other hyper-parameters were set default (in Matlab); fitPosterior function was used in the post-processing to obtain classification probabilities.

DT. Classifier was implemented using default parameters in Matlab.

RF. Algorithm was developed by arranging 100 DTs and via bootstrapping technique – multiple training subsets from training data were arranged by sampling with replacement. 100 learning cycles were performed, each corresponding to the training of a single DT.

Classifier training on statistically significant features

Initial training of the classifiers was performed using statistically significant features for the differentiation between LP and MCT, LP and STS as well as MCT and STS tissues (Fig. 1). The data, obtained from US and WL images (for WL, the set, WL1) was used. Statistically significant features were determined using non-parametric Mann-Whitney U test (at $p < 0.05$). For US imaging for the pair of LP vs. MCT—all features were significantly different; for LP vs. STS pair—similarly—all; for MCT vs. STS pair—1, 2, 4, 5, 6, 8, 10, 11, 12 features. For WL imaging for the pair of LP vs. MCT—all; LP vs. STS—all; MCT vs. STS—1, 2, 3, 4, 5, 7, 9, 10.

The extracted features were used to train LDA, SVM and DT classifiers. Initially, the classifiers were tested for possible under-fitting using resubstitution of the samples. Subsequently, the classification efficiency was evaluated using 2-fold cross-validation (1/2 of samples were used for training and 1/2 samples were left for testing), 3-fold cross-validation (2/3 for training and 1/3 for testing), 5-fold cross-validation (4/5 for training and 1/5 for testing) and 10-fold cross-validation (9/10 for training and 1/10 for testing). The results of each classification metric are presented as mean ± standard error of mean (SEM), in overall, for 2-, 3-, 5- and 10-fold cross-validations (Fig. 5).

Classifier training on optimal features

Eventually, the training of classifiers was performed in combination with the application of sequential feature addition, used to select the optimal set of features, resulting in the highest classification accuracy. For the first evaluation the initial dataset was composed by combining truly benign LPs with another set, consisting of MCTs, ranging from low to high malignancy potential, and malignant STSs. For the second evaluation the tissues, having more similar appearance, MCT and STS, were combined into a single overall dataset. This set was divided into training/testing datasets by 5-fold partition. The function of feature optimization was coupled with cross-validation. The optimal set of features was determined according to sequential feature addition, leading to the highest accuracy. Described procedure was repeated 10 times, each corresponding to a single 5-fold cross-validation, performed on random training/testing data-splits. Randomness was specified by setting random number generator (rng) seeds from #1 to #10 (in Matlab). The overall results of each classification metric are presented as mean ± SEM, corresponding to the results of cross-validation for rng seeds #1–10 (Figs. 6 and 7).

Two comparisons (i) benign LP and combined set of MCT and STS as well as (ii) MCT and STS were performed for single mode imaging using US colormaps (Fig. 2) or optical images (Fig. 3). For WL, the set WL1, containing 12 features, and set WL2, containing the same 12-features, were combined into a single WL set to create larger dataset, that would be competitive to 72-feature US set. Eventually, the decisive opportunity was left for the optimization function to select between the features, belonging to WL1 or WL2 sets. The multimodal effect was evaluated for FL + WL (or optics, abbreviated as "OPT"), US + FL, US + WL as well as US + OPT. The classification was performed for LDA, SVM and RF classifiers; in this case DT was upgraded to RF by using 100 DTs.

The analysis of the rate of optimal feature selection for each classifier was determined using a high-performance computational workstation. The latter was powered by two Intel® Xeon® Silver 4114 CPUs (2.20 GHz frequency), equipped with 128 GB of RAM, 64-bit operating system, x64-based processor.

Classification metrics

Accuracy, specificity, sensitivity, negative predictive value (NPV) and precision (positive predictive value, PPV) metrics were evaluated to quantitatively represent the performance of classifiers. The binary marking in the comparisons was: LP (0) vs. MCT (1); LP (0) vs. STS (1); MCT (0) vs. STS (1); benign LP (0) vs. combined set of MCT and STS tumors (1).

Statistical analysis

Data are presented as the mean ± SEM. Statistical significance between single and multimodal groups was evaluated using Mann-Whitney U test. The minimal level of statistical significance (p) was set to $p < 0.05$, otherwise the difference between groups was considered to be non-significant. Data analysis was performed using Matlab and Origin (OriginLab Co, USA) software.

Results

Histological tissue analysis

Figure 4A illustrates a well-differentiated lipoma—a honey-comb structured mass, composed of mature adipocyte cells. They have a typical appearance of large cells with peripherally located nuclei and lipid-abundant vacuoles. The absence of mitotic activity, cellular atypia as well as a lack of immune cell infiltration confirms the benign nature of the tissue.

Figure 4B1 and B2 represent MCT tissue, composed of round and oval cells, distributed in clusters. Mastocytes are distributed uniformly, characterised by centrally positioned nuclei. A few infiltrating eosinophils are scattered among the mast cells—a common characteristic of MCT tissue. At higher magnification (Fig. 4B2), the cytoplasmic granules of mast cells become more apparent, suggesting a well-differentiated MCT. The nuclei show rare mitotic figures. The overall low mitotic activity and absence of significant atypia indicate a benign to low-grade malignancy.

Figure 4C1–C3 illustrate the morphological structure of a high-grade STS. It is dense unencapsulated neoplasm infiltrating surrounding connective tissue (Fig. 4C1). The stroma is variable but includes areas of collagen deposition and vascular proliferation. Spindle-shaped tumor cells exhibit elongated hyperchromatic nuclei with moderate to marked nuclear pleomorphism (Fig. 4C2). Mitotic figures are frequent, including atypical forms, suggesting a high proliferative index. Occasional areas of necrosis or hemorrhage are present. Cells show nuclear enlargement, mitotic activity and disorganized architecture (Fig. 4C3). The features indicate a high-grade malignancy.

Tumor differentiation using the set of statistically significant features

Classification efficiency between LP and MCT, LP and STS as well as MCT and STS tumors using statistically significant features is presented in Fig. 5. This part of the study had followed the protocol, illustrated in Fig. 1.

For the differentiation between LP and MCT as well as LP and STS tissues, the metrics of accuracy, specificity, sensitivity, NPV and precision, in all the cases, surpassed 90% for US and resulted in ~ 100% for WL. Multimodal approach (US + WL) for LDA and DT, also, resulted in almost 100% classification efficiency. However, SVM classifier performed worse, indicating that less efficient US introduced ambiguities to the information provided by WL. On the contrary, when differentiating between two heterogeneous and more similar tissues, MCT and STS, the highest classification efficiency was determined for SVM classifier: 60–70% for US, > 70% for WL and 75–80% for US + WL. Furthermore, SVM has been evaluated positive for multimodality—statistical significance has been determined for all the classification metrics, obtained when comparing WL and US + WL groups (Table 1). This implies that multimodal approach is more beneficial for the differentiation of heterogeneous

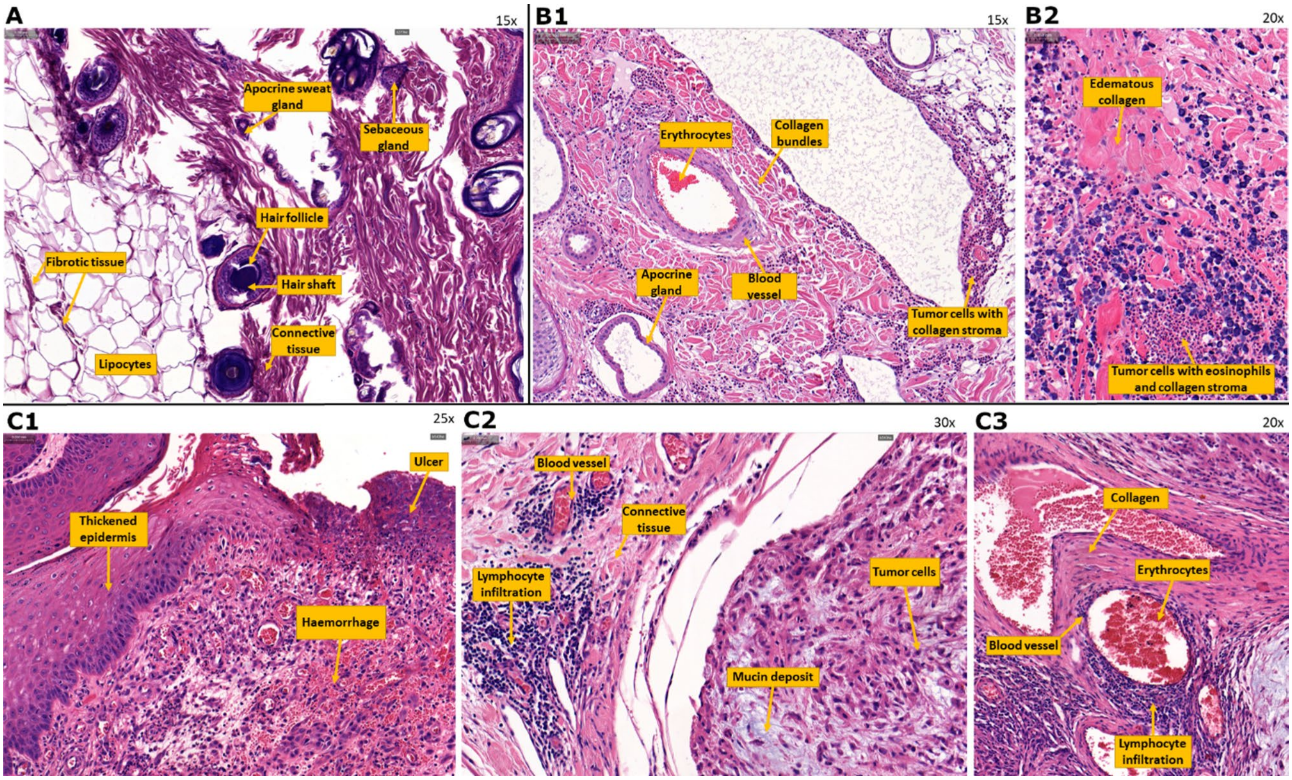

Fig. 4. Histological characteristics under white light (WL) imaging for LP (A), MCT (B1–B2) and STS tissues (C1–C3). Subplots at varying magnifications highlight detailed morphological structures within each tissue type. Textboxes annotate key histological features characteristic of each tissue class.

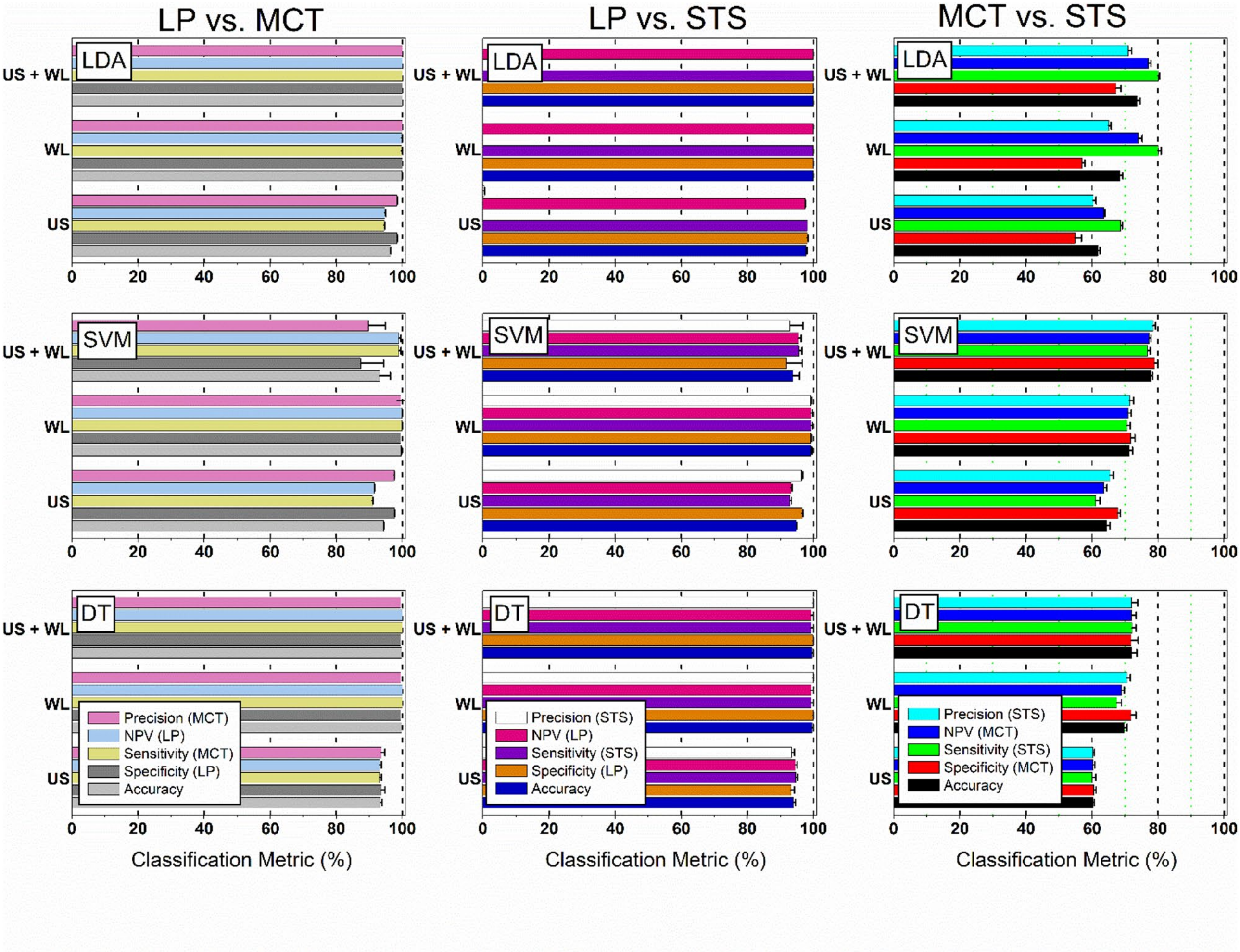

Fig. 5. Results of the differentiation between LP and MCT, LP and STS as well as MCT and STS tumors. Classification metrics are presented for LDA (upper panel), SVM (middle panel) and DT (lower panel) classifiers. Classification was performed using the set of statistically significant features, obtained from WL and US images.

	Accuracy	Specificity (MCT)	Sensitivity (STS)	NPV (MCT)	Precision (STS)
LDA US + WL vs. WL	*	*	NS	NS	*
SVM US + WL vs. WL	*	*	*	*	*
DT US + WL vs. WL	NS	NS	NS	NS	NS

Table 1. The levels of statistical significance for the metrics, obtained for the differentiation between MCT and STS tissues for US + WL and WL groups. Notations: * indicates $p < 0.05$ and NS—non-significant (Mann-Whitney U test).

tissues, MCT and STS, which are characterized by more similar visual appearance. However, when differentiating very distinct LPs from MCTs or STSs, the multimodality was not determined to be a requisite.

Tumor differentiation using the set of optimal features

LP vs. combined set of MCT and STS tissues

Comparison of classification efficiency of benign LP and combined set of MCT and STS tumors was performed after the selection of optimal set of features for US estimates: (i) Attenuation, (ii) FFT data (Peak FFT Freq and Amp), (iii) TEMP Amp data (Peak and Min TEMP Amp), (iv) Phase Change and (v) overall US data (Fig. 6, left panel). The similar approach was implemented for optical modalities: (i) FL, (ii) WL and (iii) FL + WL (OPT), as well as combined hybrid approaches (Fig. 6, right panel).

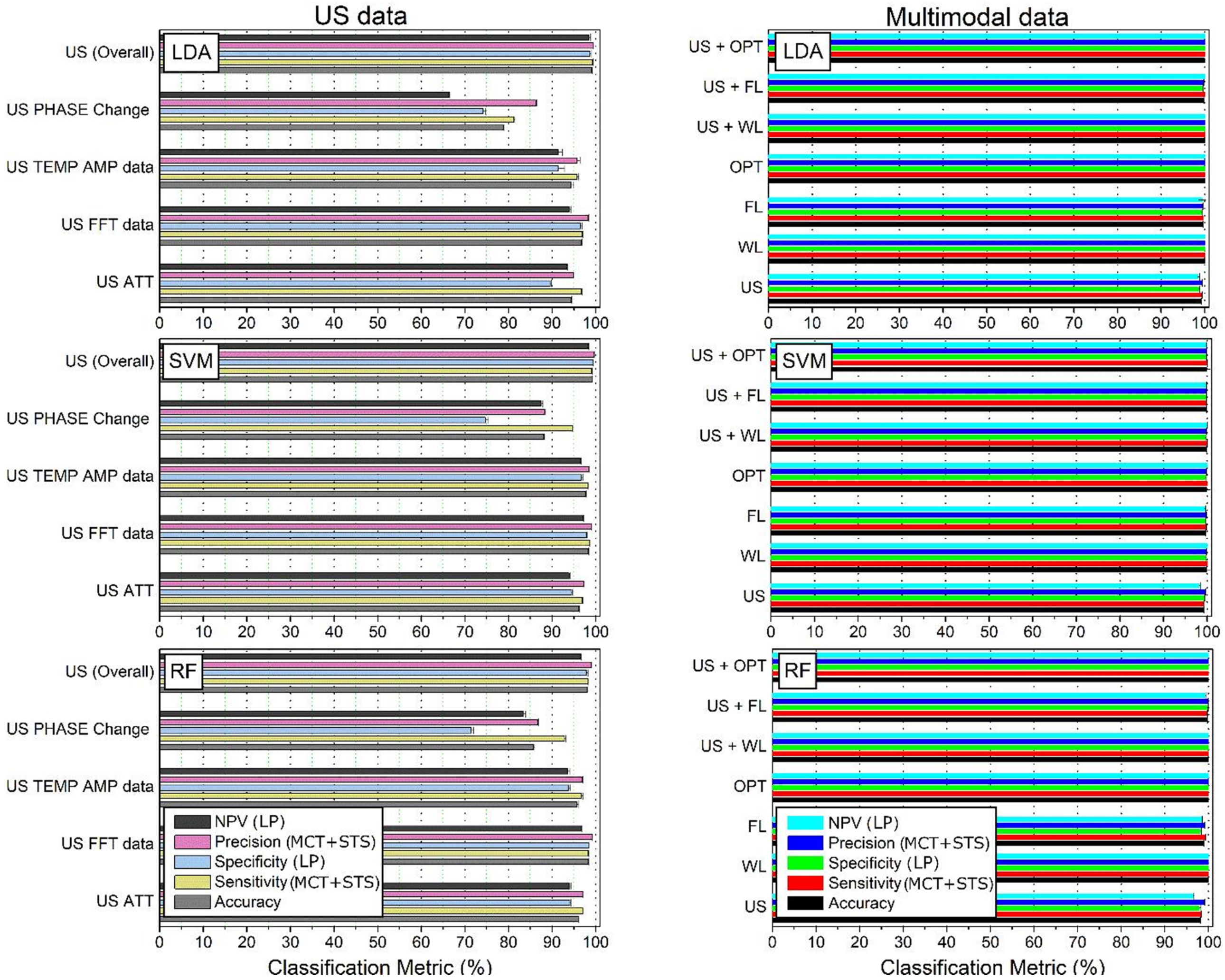

Fig. 6. Results for the differentiation between benign LP and combined set of MCT and STS tumors using US data (left panel) or optical and multimodal data (right panel). Classification metrics are presented for LDA (upper panel), SVM (middle panel) and RF (lower panel) classifiers. Metrics, related to US imaging (left panel), were acquired after performing separate feature optimization using: 12 features for: (i) US Attenuation or (ii) Phase Change; similarly, using: (iii) 24 features of US FFT data or iv) US TEMP Amp data; as well as, using: (v) 72 features, obtained from all US data, abbreviated as "US (overall)". Similarly, metrics, related to optical imaging (right panel) were acquired after separate feature optimization using: (i) 12 FL features, (ii) 24 WL (WL1 + WL2) features as well as 36 FL + WL (OPT) features. Eventually, metrics, related to multimodal imaging were obtained after feature optimization using: (i) 84 US + FL features, (ii) 96 US + WL features as well as (iii) 108 US + OPT features.

Classification metrics, evaluated using all US estimates, have exceeded 90%, except for Phase Change. The general optimization using all 72 US features resulted in 95–100% classification efficiency for all three classifiers (Fig. 6, left panel). Similarly, almost 100% classification efficiency was determined for WL or FL imaging as well as combined FL + WL, US + FL, US + WL and US + OPT approaches.

MCT vs. STS tissues

Classification efficiency between MCT and STS tissues was evaluated using optimal set of features for US estimates: (i) Attenuation, (ii) FFT data (Peak FFT Freq and Amp), (iii) TEMP Amp data (Peak and Min TEMP Amp), (iv) Phase Change and (v) overall US data (Fig. 7, left panel). Similar approach was implemented for optical modalities: (i) FL, (ii) WL and (iii) FL + WL, as well as combined hybrid approaches (Fig. 7, right panel).

US imaging. The highest classification efficiency for all three classifiers was achieved, after the optimization, using features, quantified using the colormaps of US Attenuation and temporal amplitudes; followed by FFT data, whereas the lowest—using Phase Change. SVM and RF classifiers performed better in comparison to LDA with accuracy, specificity, sensitivity, NPV and precision metrics falling in the range of ~ 70–80% efficiency (except for Phase Change). The optimization of SVM and RF using all 72 features, corresponding to all US colormaps, resulted in ~ 80% classification efficiency.

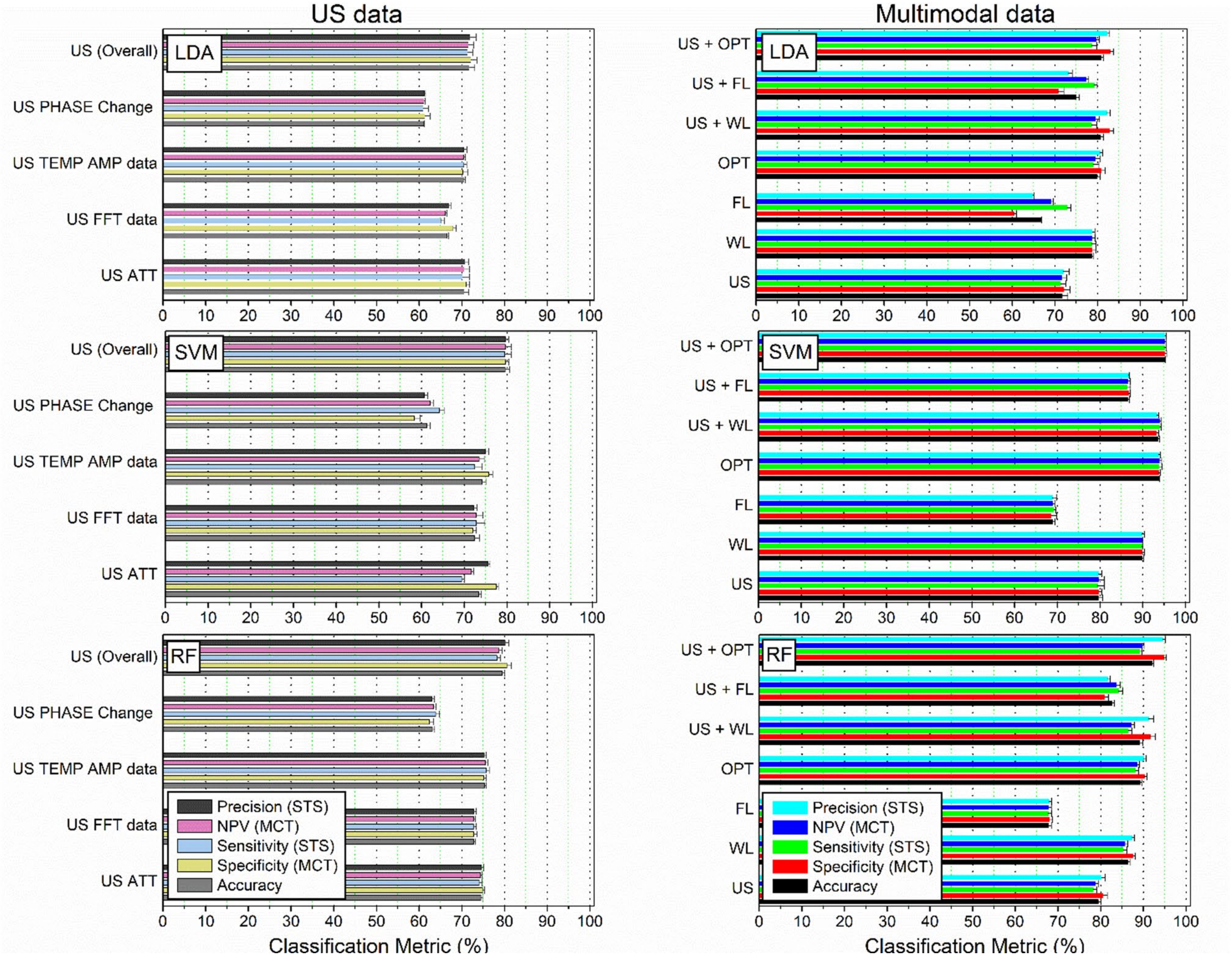

Fig. 7. Results for the differentiation between MCT and STS tumors using US data (left panel) or optical and multimodal data (right panel). Classification metrics are presented for LDA (upper panel), SVM (middle panel) and RF (lower panel) classifiers. Metrics, related to US imaging (left panel), were acquired after performing separate feature optimization using 12 features of: (i) US Attenuation or (ii) Phase Change; similarly, using: (iii) 24 features of US FFT data or (iv) US TEMP Amp data; as well as, using: (v) 72 features, obtained from all US data, abbreviated as "US (overall)". Similarly, metrics, related to optical imaging (right panel) were acquired after separate feature optimization using: (i) 12 FL features, (ii) 24 WL (WL1 + WL2) features as well as (iii) 36 FL + WL (OPT) features. Eventually, metrics, related to multimodal imaging were obtained after feature optimization using: (i) 84 features US + FL features, (ii) 96 US + WL features as well as (iii) 108 US + OPT features.

Optical imaging. The classification efficiency for LDA classifier was determined to be the lowest not only using US but also optical (FL or WL) as well as combined approaches. In general, the classification metrics did not exceed 80%, only a few metrics were determined to surpass 80%.

For both SVM and RF algorithms, tissue classification using FL data resulted in the efficiency of ~ 70%, whereas using WL data—in ~ 90% and > 85%, respectively (Fig. 7, right panel). Combined FL + WL (OPT) imaging resulted in ~ 90% classification efficiency for RF, and ~ 95% for SVM classifier. This group was determined to have a significant multimodal increment, compared with WL, for both SVM and RF classifiers (Table 2).

The classification efficiency of US + FL and US + WL was compared to US (since FL was inferior to US) and WL, respectively. The results have shown pronounced (Fig. 7, right panel) and statistically significant increment for SVM for all the classification metrics (Table 2). The classification efficiency exceeded 85% for US + FL and reached 95% for US + WL combination for SVM. The trimodal approach was evaluated to be statistically significant for three classification metrics out of five for both SVM and RF classifiers. This implies, the effect of multimodality to be detected harder, when the number of modes exceeds two. For all the multimodal groups, SVM was more stable in classification performance, compared to RF, since, SVM classifier was evaluated with a more similar classification efficiency values for all the metrics (accuracy, specificity, sensitivity, NPV and precision).

	Accuracy	Specificity (MCT)	Sensitivity (STS)	NPV (MCT)	Precision (STS)
LDA (7 significant /20 total metrics)					
OPT vs. WL	NS	NS	NS	NS	*
US + WL vs. WL	**	**	NS	NS	**
US + FL vs. FL	*	NS	***	**	NS
US + OPT vs. OPT	NS	NS	NS	NS	NS
SVM (18 significant /20 total metrics)					
OPT vs. WL	***	***	**	***	***
US + WL vs. WL	***	**	***	***	**
US + FL vs. FL	***	***	**	**	***
US + OPT vs. OPT	**	*	NS	NS	*
RF (14 significant /20 total metrics)					
OPT vs. WL	***	**	*	**	**
US + WL vs. WL	*	**	NS	NS	**
US + FL vs. FL	**	NS	***	**	NS
US + OPT vs. OPT	**	***	NS	NS	***

Table 2. Statistical significance for the classification metrics for MCT and STS tissues. Comparisons were performed between OPT and WL, US + WL and WL, US + FL and US as well as US + OPT and OPT groups. Notations: * indicates $p < 0.05$, ** $p < 0.01$, *** $p < 0.001$ and NS—non-significant (Mann-Whitney U test).

Optimal feature analysis

The most frequently selected morphological features into the optimal set for US + OPT group, for the differentiation of MCT and STS, are shown in Fig. 8 (upper left panel). The description of each feature, according to its number, is given in Appendix_Table_2. Due to the pronounced heterogeneity of malignant tissues, there was a high variation of features, corresponding to particular training-testing split. On the contrary, the differentiation between benign LPs and combined set of MCTs and STSs only required a few features (Fig. 8, upper right panel). This finding can be associated to homogenous textural pattern of benign LPs.

The summarized feature occurrences for each ultrasonic or optical feature subset (from #1 to #9) for US, OPT and US + OPT groups is presented in the middle panel of Fig. 8. For the differentiation between MCT and STS tissue, both US temporal amplitudes were the most dominant for SVM and RF classifiers for US + OPT group, whereas FFT Freq and Attenuation were favored by LDA. However, the least used subset was Phase Change for both SVM and RF classifiers.

Single FL was not very efficient for the classification of MCT and STS tissues resulting in ~ 70% classification efficiency for SVM or RF classifiers (Fig. 7). However, the features of FL (subset #9) were frequently selected into the optimal set for US + OPT group. This indicates that FL was capable to introduce supplementary information on tissue morphological characteristics, even though, this group was already full-filled with superior features of WL and US, present in US + WL group. As indicated by textboxes (Fig. 8, lower panel), a relevant number of US features was selected for SVM and RF algorithms for multimodal groups. This tendency indicates that ultrasonic features were competitive with optical features. On the contrary, the differentiation between benign LP and combined set of MCT and STS tissues exceptionally relied on WL features. Surprisingly, LDA and RF classifiers required only a single feature from WL set (LDA—average, RF—average or homogeneity).

Optimization rates

The highest classification efficiency as well as statistically significant multimodal increment was determined for SVM classifier, the second—for RF. However, during the optimization process, we have noticed significant difference in duration, required to optimize SVM or RF classifiers (Fig. 9). RF classifier required significantly longer time to complete single iteration, compared to SVM by 2.8–3.2 folds for benign LP and combined set of MCT and STS tissues (Fig. 9A1), as well as by 3.8–5.1 folds for MCT and STS tumors (Fig. 9A2). LDA classifier required the least amount of time but it was the least efficient.

Figures 9B1, 8C1 and B2, C2 indicate the dependence of total feature number within the optimal set and the duration, required for classifier optimization. We observe that significantly lower number of features (for SVM ≤ 6, for RF ≤ 7) and shorter duration was required to attain optimal classification for benign LPs and combined set of MCT and STS tissues (Fig. 9B1 and C1). On the contrary, the differentiation between MCT and STS for both SVM or RF classifiers required ≥ 10 features for the majority of cases. This followed with corresponding longer duration, required to complete single iteration (Fig. 9B2 and C2).

Right panel indicates the iteration completion time for different single or multimodal groups: (i) US, (ii) FL, (iii) WL, (iv) OPT, (v) US + FL, (vi) US + WL and (vii) US + OPT. The representation of the data in logarithmic scale indicates, that longer iteration completion times arrange in the successive order for LDA, SVM and RF classifiers (Fig. 9D1-F1 and D2-F2). Furthermore, Fig. 9G1-I1 and G2-I2 indicate a linear dependence between the total number of optimal features and time, required for optimization. Also, the optimization time is longer, when the optimization is performed using an initial set, having a larger number of features. Therefore, the distributions of features arrange in a consecutive order: (i) FL (12 features), (ii) WL (24), (iii) OPT (36), (iv) US (72), (v) US + FL (84), (vi) US + WL (96) and (vii) US + OPT (108). This implies that the initial feature set (total

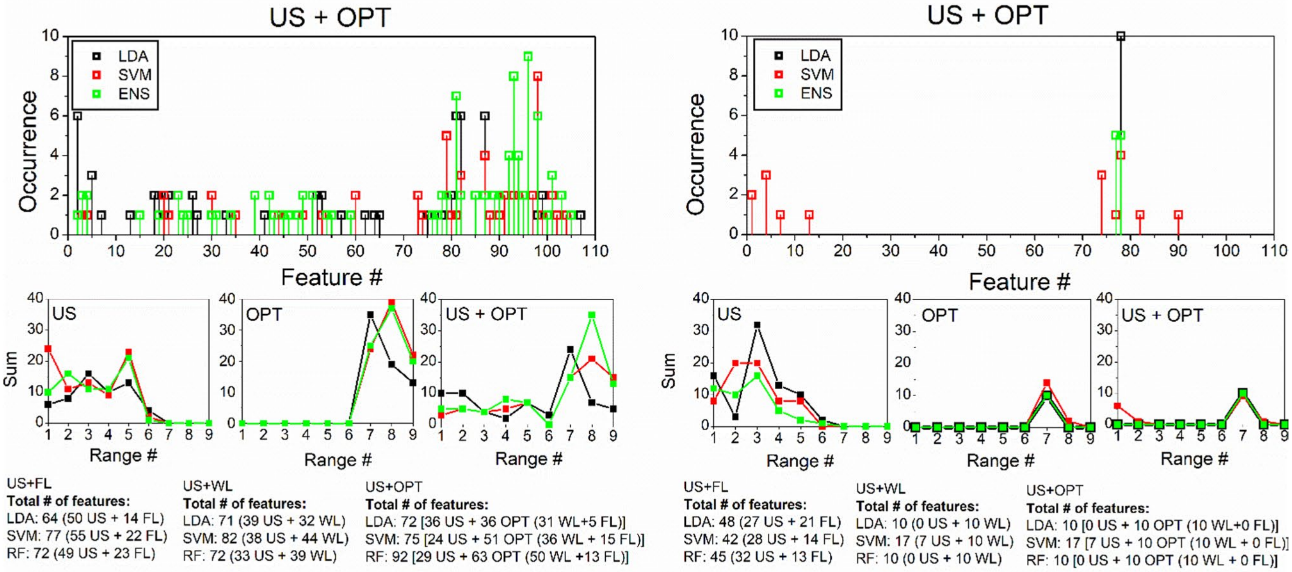

US+FL
Total # of features:
LDA: 64 (50 US + 14 FL)
SVM: 77 (55 US + 22 FL)
RF: 72 (49 US + 23 FL)

US+WL
Total # of features:
LDA: 71 (39 US + 32 WL)
SVM: 82 (38 US + 44 WL)
RF: 72 (33 US + 39 WL)

US+OPT
Total # of features:
LDA: 72 [36 US + 36 OPT (31 WL+5 FL)]
SVM: 75 [24 US + 51 OPT (36 WL + 15 FL)]
RF: 92 [29 US + 63 OPT (50 WL +13 FL)]

US+FL
Total # of features:
LDA: 48 (27 US + 21 FL)
SVM: 42 (28 US + 14 FL)
RF: 45 (32 US + 13 FL)

US+WL
Total # of features:
LDA: 10 (0 US + 10 WL)
SVM: 17 (7 US + 10 WL)
RF: 10 (0 US + 10 WL)

US+OPT
Total # of features:
LDA: 10 [0 US + 10 OPT (10 WL+0 FL)]
SVM: 17 [7 US + 10 OPT (10 WL + 0 FL)]
RF: 10 [0 US + 10 OPT (10 WL + 0 FL)]

Fig. 8. Analytical data of feature selection for the differentiation between MCT and STS (left panel) and between benign LP and combined set of MCT and STS tumors (right panel). The most frequently selected individual features into the optimal set for US + OPT group (upper panel). Summarized occurrences of features within subsets for US, OPT and US + OPT groups (middle panel); subsets: #1- Peak FFT Freq; #2- Attenuation; #3- Peak FFT Amp; #4- Peak Temp Amp; #5- Min Temp Amp; #6- Phase Change; #7 and #8- WL1 and WL2; #9- FL. Textboxes, indicating the number of US and FL and/or WL features for multimodal groups (lower panel).

number of features), subjected for the optimization, can be arranged according to the performance capabilities of the available machinery and controlled in linear dependence.

In overall, SVM classifier was evaluated to be the most efficient, based on these criteria: (i) higher number of detected significant multimodal increments between multimodal groups and (ii) being 3–5 times faster than RF algorithm, composed of 100 DTs.

Discussion

Current study underscores the value of multimodal imaging and ML in the integrative analysis of canine/feline (sub-)cutaneous neoplasms. The innovative aspect of our study is to integrate three cost-effective clinical diagnostic methods. Therefore, single (US, FL and WL) and bi-modal (US + FL, US + WL and OPT) as well as tri-modal (US + OPT) imaging combinations were analyzed. Subsequently, the integration of ML algorithms with optical and US data was performed to validate multimodal imaging technology on clinical ex vivo samples. LP, MCT and STS exhibited inherent tissue characteristics, corresponding to the distinct nature of their pathogenesis. Compared to homogeneous benign LP, MCT and STS tissues displayed heterogeneous texture, irregular tumor margins as well as pronounced vascularization. All these properties are indicative of enhanced malignant potential of MCTs and STSs.

WL imaging is conventionally used for its ability to provide initial assessment of tumor histological slides at high-resolution. However, it is limited only to superficial inspection, which restricts its effectiveness for visualizing deeper structures within the tissues[22]. In our study, WL imaging resulted in the classification efficiency of ~ 100% for the differentiation between benign LP and combined set of MCT and STS tissues for all

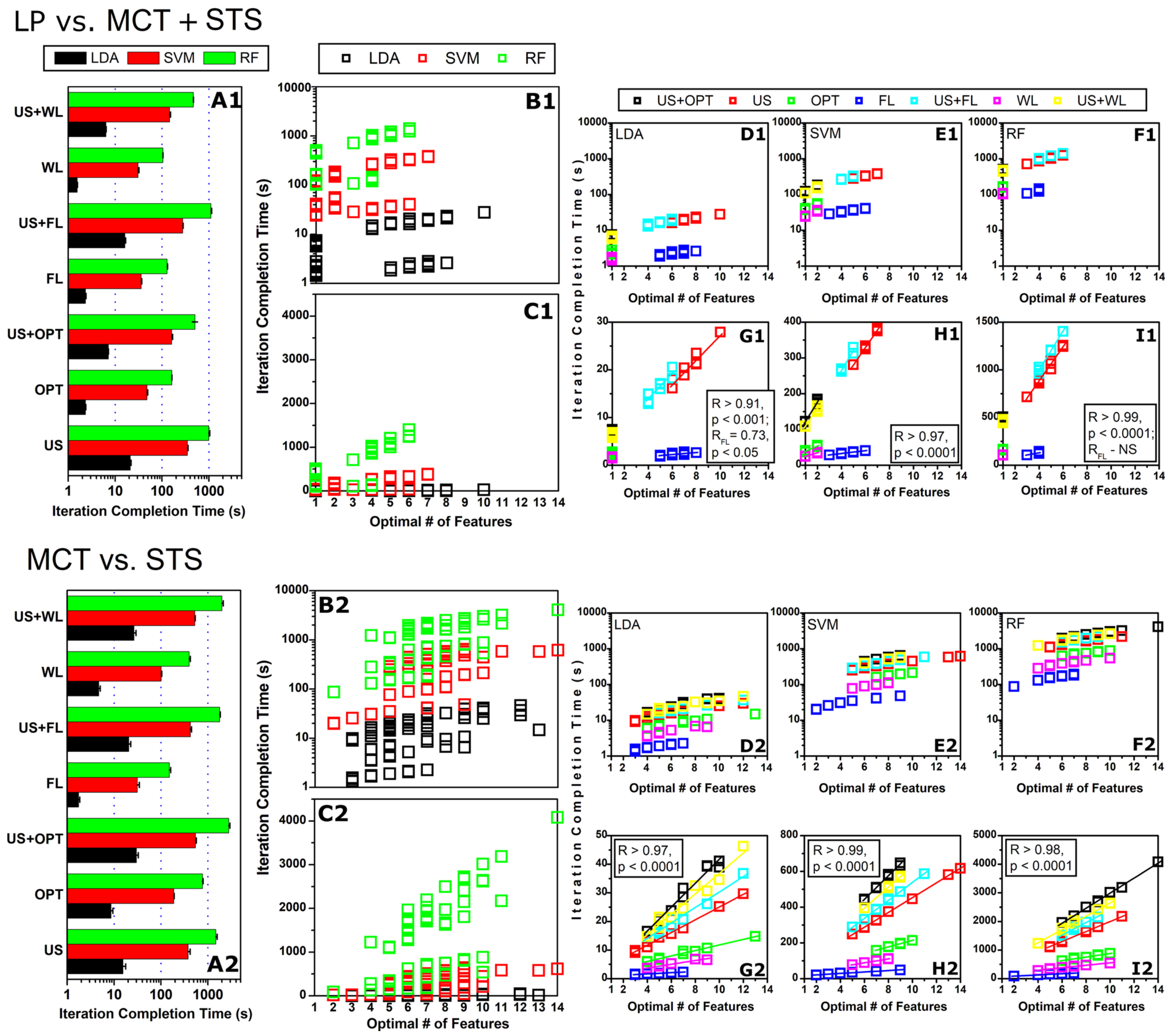

Fig. 9. Analysis of the duration, required for optimal feature selection for LDA, SVM and RF classifiers for the differentiation between benign LP and combined set of MCT and STS (A1) as well as between MCT and STS tissues (A2). The dependence of total feature number (within optimal feature set) and iteration completion time, required for optimal feature selection for benign LP and combined set of MCT and STS (B1 and C1) as well as for MCT and STS (B2, C2) tumors. Iteration completion time for different single groups: (i) US, (ii) FL, (iii) WL, or multimodal groups: (iv) OPT, (v) US + FL, (vi) US + WL and (vii) US + OPT for the differentiation between benign LP and combined set of MCT and STS (D1-I1) as well as for MCT and STS (D2-I2) tissues. Strong linear dependence ($R > 0.91$, $p < 0.001$) was determined between total number of optimal features and iteration completion time for the majority of cases, except for FL group for LDA ($R = 0.73$, $p < 0.05$) and RF (non-significant, NS) classifiers. Notations: R—correlation coefficient, p—significance level.

classifiers (Fig. 6). For the differentiation between MCT and STS tumors, it resulted in classification efficiency: <80% for LDA, ~90% for SVM and >85% for RF, respectively (Fig. 7).

FL imaging highlights specific intra- and/or sub-cellular structures, thus, enhancing the detection of malignant tissues[23]. In the current study, we implemented label-free FL imaging, which resulted in the classification efficiency of ~100% for the differentiation of benign LP and combined set of MCT and STS tumors for all the classifiers (Fig. 6). However, for the differentiation between MCT and STS tissues, single FL imaging resulted only in ~70% classification efficiency for SVM classifier (Fig. 7). Subsequently, our research aimed to use FL imaging as an additional technique in multimodal classification.

High-frequency US imaging complements optical techniques by providing real-time non-invasive visualization of deeper regions, located within the tissue[24]. In our study, high frequency US was effectively exploited for structural characterization of tissues and optically non-transparent deeper regions. Single US imaging resulted in the classification efficiency of ~100% for benign LP and combined set of MCT and STS tissues for all classifiers (Fig. 6). For the differentiation between MCT and STS tissues, the highest classification efficiency using US data was obtained ~ 80%, when optimized from all 72 US features using SVM and RF classifiers (Fig. 7).

When using statistically significant features, we have observed multimodal increment for all the classification metrics (accuracy, specificity, sensitivity, NPV and precision) for the group of US + WL (compared to WL) only for SVM classifier. The other classifiers, LDA and DT, did not result in significant increase when tested for multimodality (Table 1).

Eventually, after combining US and optical imaging data, we have performed bi-modal as well as tri-modal evaluation of multimodality (Figs. 6 and 7). The obtained hybrid combinations were: FL + WL, US + FL, US + WL and US + OPT. Statistically significant multimodal increment was observed for bimodal combinations of FL + WL, US + FL, US + WL for SVM classifier ($p < 0.01$) for all the classification metrics (accuracy, specificity, sensitivity, NPV and precision). However, trimodal combination failed to increase significantly. Other classifiers were less efficient in producing multimodal increment—only RF achieved relevant increase in all classification metrics for FL + WL group compared to WL (Table 2).

ML algorithms can detect complex patterns and features not apparent for the human eye. However, ML applications in veterinary cancer are poorly investigated[8,25–28]. ML models can be coupled and integrated with clinical decision support systems with the aim to provide cancer diagnosis. In the current approach, we have explored LDA, SVM and RF classifiers. The highest classification efficiency between MCT and STS tumors as well as the most relevant multimodal effect was determined for SVM classifier (~ 95%) (Fig. 7). What is more, compared on the average iteration time SVM was up to 5 folds faster than RF algorithm (Fig. 9), which was the second in classification efficiency. Indeed, SVM as the most efficient classifier was also reported by Tiwari et al.[19]. Researchers performed similar study with the purpose to differentiate between human (sub-)cutaneous melanoma tumors and melanocytic naevi.

Various strategies have been reported for the determination of relevant feature set for ML-based tissue differentiation. A very popular approach in the field is to apply the set of statistically significant features[8,19,29–33]. SVM, trained on statistically significant features, showed a relevant multimodal increment between WL and US + WL groups (Fig. 5; Table 1). However, much higher classification efficiency (~ 95%) was obtained when performing the optimization via sequential features addition from a large feature dataset (Fig. 7; Table 2). This indicates that some non-significant features may be valuable for differentiating such heterogeneous tissues, as MCT and STS, especially at specific training/testing partitions. Indeed, FL was less-efficient, when used for the classification of MCT and STS tumors alone (< 70%). However, despite being inferior to US or WL in classification efficiency, FL features were competitive to US and WL, when feature optimization was performed for US + FL as well as US + OPT groups (Fig. 8). In addition, another valuable insight within multimodality can be observed from Fig. 8. Total number of features remains approximately the same for single WL or OPT group, compared to respective multimodal US + WL or US + OPT groups, for SVM classifier. And since, multimodal increment is identified as positive, this feature rearrangement implies that US features are capable of substituting highly-efficient WL or OPT features, not only be added. Therefore, the optimization function free-willingly selects US features, identifying them as valuable, although they are inferior compared to superior WL features.

Data form this study indicates that our approach of tri-modal diagnostics, incorporating US, FL and WL imaging, is capable to provide diagnostic accuracy > 95% between heterogeneous cancer types such as MCT and STS. The latter are often difficult to differentiate due to overlapping histological features and intra-class heterogeneity. Notably, current classification efficiency even surpassed the results, achieved using bi-modal OCT-Raman approach on canine/ feline (sub-)cutaneous tumors[8]. The latter study, incorporating high-cost instrumentation, reported malignant tumor detection specificity and sensitivity of 97.7 and 93.9%, respectively. In contrast, our current approach achieved ~ 100% efficiency between LP and combined MCT and STS set. While both are powerful techniques, the cost of their implementation are high: OCT typically surpasses 70000 EUR, and Raman system can exceed 100 000 EUR, depending on the integration and configuration[34,35]. Our approach utilizes affordable techniques of optical imaging (WL and FL), that can be performed using slide-scanners, common for laboratories. However, we acknowledge that our high-frequency US imaging system is priced comparably to OCT. To compensate for this, cheaper conventionally used B-scan echoscopes could be employed for the evaluation of resected tumors.

Nevertheless, our multimodal approach offers the following superiorities: (i) considerably higher diagnostic accuracy, (ii) ML-provided automation, as well as (iii) a more versatile multimodal setup, that can be efficiently incorporated into conventional tissue assessment workflows. Unlike OCT, which can work on freshly resected tissue, our method requires to prepare histological slides. However, the increase in classification accuracy and low cost, from using WL and FL imaging instruments, surpasses the time, required for sample preparation, especially, for those cases, where real-time imaging, is not in demand.

Indeed, developed method would be mostly beneficial for veterinary laboratories, that are already working with histological samples, offering diagnostic support for veterinary histopathologist. If the discrepancy between ML- and human-derived diagnosis occurs, the unclear cases can be double checked by human. Thus, eventually, our framework could become a reliable diagnostic technique, efficiently assisting veterinary oncologists. Also, we recognize the limitations to be addressed in our future studies: (i) validation of obtained results on a larger cohorts of individuals in clinical settings, as well as (ii) integration of automatic margin selection algorithm, so that only intra-marginal area with cancer tissue would be used for tissue classification. Currently, our study demonstrates the feasibility to differentiate between heterogeneous veterinary (sub-)cutaneous MCT and STS tumors using a bi- or tri-modal combination of US, WL and FL imaging, leading to classification accuracy exceeding 95%.

Conclusions

Current study evaluates the feasibility of multimodal imaging and machine learning for the differentiation of canine/feline (sub-)cutaneous tumors, lipomas, mastocytomas and soft tissue sarcomas. The innovative aspect of our study is to integrate three cost-effective clinical diagnostic methods, ultrasound, autofluorescence and white light imaging Research resulted in ~ 100% classification efficiency between benign lipomas and combined set of semi-malignant MCT and malignant STS tissues for linear discriminant analysis, support vector machine and random forest classifiers.

For the differentiation between mastocytoma and sarcoma tumors, support vector machine classifier showed significant ($p < 0.05$) multimodal effect using both statistically significant set of features as well as optimal set of features, determined using sequential feature addition. Resulting classification efficiency was > 85% for ultrasound + fluorescence and ~ 95% for ultrasound + white light or ultrasound + optics multimodal approaches.

Both support vector machine and random forest algorithms outperformed conventional linear discriminate analysis classifier for the differentiation of heterogeneous mastocytomas and soft tissue sarcoma.; Support vector machine classifier was able to detect significant ($p < 0.05$) multimodal effect in bimodal fluorescence + white light, ultrasound + fluorescence and ultrasound + white light groups; whereas random forest algorithm only for fluorescence + white light.

For both classifiers multimodality was less observed in trimodal combination of ultrasound + optics, indicating that addition of modes has the upper limit of the accuracy increase.

Multimodal approach is more beneficial for the differentiation of heterogeneous tissues, MCT and STS, which are characterized by more similar visual appearance. However, when differentiating very distinct LPs from MCTs or STSs, the multimodality is not a requisite.

Inferior ultrasound or fluorescence features are, indeed, competitive with the features of superior white light, and are selected during the process of sequential optimization. Furthermore, in multimodal groups, ultrasound features tend to substitute the features of white light, not just simply be added. This can be considered as the manifestation of multimodal effect even, if the increase in classification metrics remains the same.

Proposed multimodal technique would be mostly beneficial for veterinary cancer laboratories, already working with histological samples. It would become a reliable diagnostic support for veterinary histopathologist. If a discrepancy between machine- and human-derived diagnosis is determined, the unclear cases can be double inspected by human.

Received: 17 December 2024; Accepted: 15 May 2025

References

1. Hauck, L. Tumors of the skin and subcutaneous tissues, 5th edn. In *Withrow & MacEwen's Small Animal Clinical Oncology* (eds Withrow, S., Vail, D. & Page, R.) 375–401 (Saunders WB, 2013).
2. Blackwood, L. et al. European consensus document on mast cell tumours in dogs and cats. *Vet. Comp. Oncol.* **10** (3), e1–e29. https://doi.org/10.1111/j.1476-5829.2012.00341.x (2012).
3. Withrow, S. J. & Vail, D. M. Withrow and MacEwen's Small Animal Clinical Oncology-E-Book (Elsevier Health Sciences, 2019).
4. Lages, M. & Selmic, L. E. Exploring optical coherence tomography imaging depth to differentiate tissues at surgical margins. *Vet. Comp. Oncol.* **19** (4), 763–769. https://doi.org/10.1111/vco.12745 (2021).
5. Wang, S. L., Lee, J. J. & Liao, A. T. Comparison of cytological and histopathological validation on fine needle aspiration of superficial masses. *Taiwan. Vet. J.* **40**, 191–198. https://doi.org/10.1142/S168264851450022X (2014).
6. Selmic, L. E. & Ruple, A. A systematic review of surgical margins utilized for removal of cutaneous mast cell tumors in dogs. *BMC Vet. Res.* **16** (1), 5. https://doi.org/10.1186/s12917-019-2227-8 (2020).
7. Coleman, M. J. et al. Diagnostic accuracy of optical coherence tomography for surgical margin assessment of feline injection-site sarcoma. *Vet. Comp. Oncol.* **19** (4), 632–640. https://doi.org/10.1111/vco.12766 (2021).
8. Tamošiūnas, M. et al. Multimodal approach of optical coherence tomography and Raman spectroscopy can improve differentiating benign and malignant skin tumors in animal patients. *Cancers (Basel).* **14** (12), 2820. https://doi.org/10.3390/cancers14122820 (2022).
9. Selmic, L. E. et al. Intra-operative imaging of surgical margins of canine soft tissue sarcoma using optical coherence tomography. *Vet. Comp. Oncol.* **17** (1), 80–88. https://doi.org/10.1111/vco.12448 (2019).
10. Ohlerth, S. & O'Brien, R. T. Contrast ultrasound: General principles and veterinary clinical applications. *Vet. J.* **174**, 501–512 (2007).
11. Longo, M. et al. Real-time elastosonography of lipomatous vs. malignant subcutaneous neoplasms in dogs: Preliminary results. *Vet. Radiol. Ultrasound.* **59**, 198–202 (2018).
12. Miura, K., Nasu, H. & Yamamoto, S. Scanning acoustic microscopy for characterization of neoplastic and inflammatory lesions of lymph nodes. *Sci. Rep.* **3**, 1255. https://doi.org/10.1038/srep01255 (2013).
13. Akhtar, R., Cruickshank, J. K., Zhao, X., Derby, B. & Weber, T. A pilot study of scanning acoustic microscopy as a tool for measuring arterial stiffness in aortic biopsies. *Artery Res.* **13**, 1–5. https://doi.org/10.1016/j.artres.2015.11.001 (2016).
14. Lahiani, A., Klaiman, E. & Grimm, O. Enabling histopathological annotations on immunofluorescent images through virtualization of hematoxylin and Eosin. *J. Pathol. Inf.* **9**, 1. https://doi.org/10.4103/jpi.jpi_61_17 (2018).
15. Fischer, A. H., Jacobson, K. A., Rose, J. & Zeller, R. Hematoxylin and Eosin staining of tissue and cell sections. *CSH Protoc.* https://doi.org/10.1101/pdb.prot4986 (2008).
16. Narayanan, S. et al. Bimodal multispectral imaging system with cloud-based machine learning algorithm for real-time screening and detection of oral potentially malignant lesions and biopsy guidance. *J. Biomed. Opt.* **26** (8), 086003. https://doi.org/10.1117/1.JBO.26.8.086003 (2021).
17. Wu, J. et al. Multimodal microscopic imaging with deep learning for highly effective diagnosis of breast cancer. *Opt. Lasers Eng.* **168**, 107667. https://doi.org/10.1016/j.optlaseng.2023.107667 (2023).
18. Gesperger, J. et al. Improved diagnostic imaging of brain tumors by multimodal microscopy and deep learning. *Cancers (Basel).* **12** (7), 1806. https://doi.org/10.3390/cancers12071806 (2020).
19. Tiwari, K. A., Raišutis, R., Liutkus, J. & Valiukevičienė, S. Diagnostics of melanocytic skin tumours by a combination of ultrasonic, dermatoscopic and spectrophotometric image parameters. *Diagnostics (Basel).* **10** (9), 632. https://doi.org/10.3390/diagnostics10090632 (2020).

20. Echegaray, S., Bakr, S., Rubin, D. L. & Napel, S. Quantitative image feature engine (QIFE): An open-source, modular engine for 3D quantitative feature extraction from volumetric medical images. *J. Digit. Imaging*. **31** (4), 403–414. https://doi.org/10.1007/s10278-017-0019-x (2018).
21. Haralick, R. M., Robert, M., Shanmugam, K. & Dinstein, I. Textural features for image classification. *IEEE Trans. Syst. Man. Cybern.*. **SMC-3** (6), 610–621. https://doi.org/10.1109/TSMC.1973.4309314 (1973).
22. Farahani, N., Parwani, A. & Pantanowitz, L. Whole slide imaging in pathology: Advantages, limitations, and emerging perspectives. *Pathol. Lab. Med. Int.* **7**, 23–33. https://doi.org/10.2147/PLMI.S59826 (2015).
23. Zhang, Y., Kang, L., Yu, W., Tsang, V. T. C. & Wong, T. T. W. Three-dimensional label-free histological imaging of whole organs by microtomy-assisted autofluorescence tomography. *iScience* **25** (1), 103721. https://doi.org/10.1016/j.isci.2021.103721 (2022).
24. Wang Xl, Lin, S. & Lyu, G. Advances in the clinical application of ultrasound elastography in uterine imaging. *Insights Imaging*. **13**, 141. https://doi.org/10.1186/s13244-022-01274-9 (2022).
25. Mesa, K. J. et al. Intraoperative optical coherence tomography for soft tissue sarcoma differentiation and margin identification. *Lasers Surg. Med.* **49** (3), 240–248. https://doi.org/10.1002/lsm.22633 (2017).
26. Ye, Y., Sun, W. W., Xu, R. X., Selmic, L. E. & Sun, M. Intraoperative assessment of canine soft tissue sarcoma by deep learning enhanced optical coherence tomography. *Vet. Comp. Oncol.* **19** (4), 624–631. https://doi.org/10.1111/vco.12747 (2021).
27. Dank, G. et al. A pilot study for a non-invasive system for detection of malignancy in canine subcutaneous and cutaneous masses using machine learning. *Front. Vet. Sci.* **10**, 1109188. https://doi.org/10.3389/fvets.2023.1109188 (2023).
28. Zuraw, A. & Aeffner, F. Whole-slide imaging, tissue image analysis, and artificial intelligence in veterinary pathology: An updated introduction and review. *Vet. Pathol.* **59** (1), 6–25. https://doi.org/10.1177/03009858211040484 (2022).
29. Khanna, P., Sahu, M. & Machine Learning. in *Advances in Signal Processing, Embedded Systems and IoT*. Lecture Notes in Electrical Engineering Vol. 992 (eds Chakravarthy, V., Bhateja, V., Flores Fuentes, W., Anguera, J. & Vasavi, K. P.) (Springer, 2023). https://doi.org/10.1007/978-981-19-8865-3_26Performance Analysis of Breast Cancer Data Using Mann–Whitney U Test and.
30. Deng, Z. et al. Ultrasound-based radiomics machine learning models for diagnosing cervical lymph node metastasis in patients with non-small cell lung cancer: A multicentre study. *BMC Cancer*. **24**, 536. https://doi.org/10.1186/s12885-024-12306-6 (2024).
31. Sharma, A. & Rani, R. A systematic review of applications of machine learning in Cancer prediction and diagnosis. *Arch. Computat Methods Eng.* **28**, 4875–4896. https://doi.org/10.1007/s11831-021-09556-z (2021).
32. Andrėkutė, K., Linkevičiūtė, G., Raišutis, R., Valiukevičienė, S. & Makštienė, J. Automatic differential diagnosis of melanocytic skin tumors using ultrasound data. *Ultrasound Med. Biol.* **42** (12), 2834–2843. https://doi.org/10.1016/j.ultrasmedbio.2016.07.026 (2016).
33. Andrekute, K. et al. Automated Estimation of melanocytic skin tumor thickness by ultrasonic radiofrequency data. *J. Ultrasound Med.* **35** (5), 857–865. https://doi.org/10.7863/ultra.15.02051 (2016).
34. Izatt, J. A. & Choma, M. A. Theory of optical coherence tomography. In: Optical Coherence Tomography. Biological and Medical Physics, Biomedical Engineering (eds Drexler, W. & Fujimoto, J. G). Springer, Berlin. https://doi.org/10.1007/978-3-540-77550-8_2 (2008).
35. Kong, K., Kendall, C., Stone, N. & Notingher, I. Raman spectroscopy for medical diagnostics–From in-vitro biofluid assays to in-vivo cancer detection. *Adv. Drug Deliv Rev.* **89**, 121–134. https://doi.org/10.1016/j.addr.2015.03.009 (2015).

Author contributions

MM: conceptualization; methodology; investigation; data curation; formal analysis; visualization; writing - original draft; writing - review and editing; GR: conceptualization; methodology; data curation; formal analysis; RR: conceptualization; investigation; funding acquisition; writing - editing; BC: methodology; data curation; MT: conceptualization; methodology; funding acquisition; supervision; writing - editing.

Funding

This work was supported by a grant (S-MIP-23-81) “Diagnostic assessment of machine learning algorithms for non-invasive multimodal imaging-based classification of canine and feline skin cancer” (Research Council of Lithuania). Also, the research was funded by the Latvian Council of Science, project LZP-2022/1-0274 “Histological recognition and analysis of veterinary tumors surgical margins by using artificial intelligence and multimodal imaging”.

Declarations

Ethics approval and consent to participate

Permission No. DZLAEP-2021/3 of the Ethical Council of Animal Welfare and Protection (Latvia University of Life Sciences and Technologies, Jelgava, Latvia).

Competing interests

The authors declare no competing interests.

Additional information

Supplementary Information The online version contains supplementary material available at https://doi.org/10.1038/s41598-025-02668-7.

Correspondence and requests for materials should be addressed to M.M. or G.R.